The near field, Westervelt far field, and inverse-law far field of the audio sound generated by parametric array loudspeakers

Jiaxin Zhong[1a)], Ray Kirby[1], Xiaojun Qiu[1]

[1] Centre for Audio, Acoustics and Vibration, Faculty of Engineering and Information Technology, University of Technology Sydney, New South Wales 2007, Australia

Abstract

The near and far fields of traditional loudspeakers are differentiated by whether the sound pressure amplitude is inversely proportional to the propagating distance. However, the audio sound field generated by a parametric array loudspeaker (PAL) is more complicated, and in this article it is proposed to be divided into 3 regions: near field, Westervelt far field, and inverse-law far field. In the near field, the audio sound experiences strong local effects and an efficient quasilinear solution is presented. In the Westervelt far field, local effects are negligible so that the Westervelt equation is used, and in the inverse-law far field a simpler solution is adopted. It is found that the boundary between the near and Westervelt far fields for audio sound lies at approximately $a^2/\lambda - \lambda/4$, where a is transducer radius and λ is ultrasonic wavelength. At large transducer radii and high ultrasonic frequencies, the boundary moves close to the PAL and can be estimated by a closed-form formula. The inverse-law holds for audio sound in the inverse-law far field and is more than 10 meters away from the PAL in most cases. With the proposed classification, it is convenient to apply appropriate prediction models to different regions.

I. INTRODUCTION

Parametric array loudspeakers (PALs) generate highly directional audio sounds in air due to the nonlinear interactions of ultrasonic beams.[1] PALs have been used in audio applications such as active noise control,[2] measurement of the acoustic parameters of materials,[3] mobile robotic navigation,[4] stand-off concealed weapons detection,[5] directivity control,[6] and constructions of omni-directional loudspeakers.[7] Therefore, it is important to be able to predict the sound pressure of the audio waves generated by PALs in the full field efficiently and accurately. The near and far fields of traditional loudspeakers are differentiated by whether the sound pressure amplitude is inversely proportional to the propagating distance in the region,[8] but the audio sound fields generated by a PAL are more complicated. In this paper, it is proposed to divide the audio sound field into 3 regions: the inverse-law far field, the Westervelt far field, and a near field. With this proposed classification, appropriate models can be chosen for different regions to enable faster and more accurate sound field calculation.

In the inverse-law far field, the inverse-law holds, and the solutions are the simplest. Starting from the Lighthill equation, Westervelt obtained a closed-form formula for the audio sound in the inverse-law far field by assuming the ultrasound is collimated and nonlinear interactions of ultrasound take place only over a limited distance.[9] Berktay and Leahy modified Westervelt's formula by taking into account effects arising from the cylindrical/spherical spreading of ultrasonic waves, and they improved prediction accuracy by introducing an aperture factor for the transducer and the product directivity of ultrasonic waves.[10,11] The Berktay solution is given as a simple expression in the time domain, which provides the basis for the signal modulation techniques in the realization of PALs.[1,12] Several modifications to the Berktay model were later proposed to improve the prediction accuracy for the sidelobes of PALs.[13] A more accurate model has been proposed which employs the convolution of the Westervelt directivity and the ultrasonic wave directivities.[14-17] Although the ultrasonic waves are not assumed as collimated in the convolution model, they are assumed to be exponentially attenuated along each direction, which is not true in practice because of the complexity in the near field of ultrasonic transducers. The boundary of the inverse-law field is often far away from the transducer.[17]

The Westervelt far field is defined as the region where Westervelt equation is accurate and the local effects characterized by the ultrasonic Lagrangian density are negligible.[18,19] When the quasilinear approximation is assumed, the audio sound can be considered as the radiation from an infinitely large virtual volume source, with the source density proportional to the product of the ultrasonic pressure. In earlier studies, the ultrasonic beams were simply assumed to be spherically spreading with a directivity function.[16,17] Recently, the nonlinear interactions of actual ultrasonic beams generated by a transducer were modelled to improve prediction accuracy.[20,21] To simplify the calculation, the paraxial (Fresnel) approximation is usually assumed for ultrasonic waves and this enables a Gaussian beam expansion method to be used because the ultrasonic wavelength is usually much smaller than the PAL radius.[22,23] If the paraxial approximation is assumed for both ultrasonic and audio waves, then the Westervelt equation reduces to the well known Khokhlov-Zabolotskaya-Kuznetsov (KZK) equation after approximating a second order derivative of sound pressure with respect to the propagating direction by a first order derivative. The calculation is further simplified, although the result is accurate only inside the paraxial region, which is inside about 20° from the transducer axis.[24]

In the near field, the local effects characterized by the ultrasonic Lagrangian density cannot be neglected. The audio sound pressure distribution is more complicated and local maxima and minima occur in a similar way to that observed in the near field of traditional loudspeakers. The general second-order nonlinear wave equation is accurate in the modelling of the near field audio sound.[18] However, its equivalent form written in terms of the velocity potential (the Kuznetsov equation), is often used because the evaluation of the second-order spatial derivatives of the ultrasonic Lagrangian density can be avoided.[19,25] Unfortunately, the calculation of the quasilinear solution of the Kuznetsov equation is rather time-consuming, so the audio sound in the near field of PALs is rarely calculated using this equation. The audio sound in the near field of the PAL can also be obtained by using the direct numerical calculation of the Navier-Stokes equations in the time domain, although this again incurs heavy computational expenditure.[26] Thus, the near field for audio sound generated by PALs is complicated and difficult to calculate, which means that it is convenient to separate out the sound pressure field and to apply different models to different regions.

In this paper, a simplified but rigorous expression of the quasilinear solution of Kuznetsov equation for a baffled circular PAL is developed first, which is based on a spherical harmonic expansion method and this is used to calculate the audio sound in the near field. This is designed to extend the method reported in Ref. 21 by adding the ultrasonic Lagrangian density so that local effects are considered in the solution. Compared to the existing model in Ref. 19, where the five-fold integral has to be evaluated numerically, the proposed spherical expansion can be calculated efficiently without loss of accuracy. The accurate expressions for calculating the audio sounds in the Westervelt far field and the inverse-law far field are then obtained by simplifying the proposed spherical expansion. With these proposed efficient and accurate calculation methods, the transition distances among these 3 regions are then investigated quantitatively. After identifying a region an appropriate prediction model can then be chosen to enable fast and accurate calculation of the sound field for various applications.

II. METHODS

When a baffled circular PAL with a radius a generates two harmonic ultrasound waves at frequencies f_1 and f_2, with $f_1 > f_2$, the audio sound with frequency $f_a = f_1 - f_2$ is demodulated in air due to the nonlinearity. The velocity profile on the transducer surface commonly used in applications is assumed to be uniform as

$$v_0(t) = v_{1,0}\mathrm{e}^{-\mathrm{j}\omega_1 t} + v_{2,0}\mathrm{e}^{-\mathrm{j}\omega_2 t}, \tag{1}$$

where j is the imaginary unit, $v_{i,0}$ is the amplitude of the vibration velocity, and $\omega_i = 2\pi f_i$ ($i = 1$, 2) is the angular frequency of the ith primary wave. The radiation of the PAL is governed by the second-order nonlinear wave equation,[18,19]

$$\nabla^2 p - \frac{1}{c_0^2}\frac{\partial^2 p}{\partial t^2} = -\frac{\delta}{c_0^2}\nabla^2\frac{\partial p}{\partial t} - \frac{\beta}{\rho_0 c_0^4}\frac{\partial^2 p^2}{\partial t^2} - \left(\nabla^2 + \frac{1}{c_0^2}\frac{\partial^2}{\partial t^2}\right)L, \tag{2}$$

where p is the sound pressure, c_0 is the small-signal sound speed, and "second-order" means terms of third and higher orders in the acoustic variables are neglected in the derivation.[18] On the right-hand side of Eq. (2), the first term accounts for the fluid thermo-viscosity, where δ is the sound diffusivity parameter and this is related to the sound attenuation coefficient α at the angular frequency ω by $\alpha(\omega) = \omega^2\delta/(2c_0^3)$;[27] the second term accounts for the nonlinearity, where ρ_0 is the static fluid density and $\beta = 1.2$ is the nonlinearity coefficient in air; the third term characterizes the local (non-cumulative) effects where L stands for the Lagrangian density,[18,19]which is given as

$$L = \frac{1}{2}\rho_0 \mathbf{v}\cdot\mathbf{v} - \frac{p^2}{2\rho_0 c_0^2}, \tag{3}$$

where $\mathbf{v}$ is the acoustic particle velocity vector.

Equation (2) is difficult to solve directly, so different assumptions and simplifications are usually made in the mathematical modelling at different approximation levels. Two commonly used simplifications assume that local effects are negligible[18,19] and the audio sound pressure amplitude is inversely proportional to the propagating distance.[9,14] The prediction error caused by each approach depends on the distance between the field point and the PAL.[19] To further illustrate this, the audio sound field generated by a PAL is divided into 3 regions: the near field, the Westervelt far field and the inverse-law far field. In the near field, the local effects are strong so that Eq. (2) has to be used to calculate the audio sound.[19] In the Westervelt far field, these local effects are negligible so that Eq. (2) reduces to Westervelt's equation after neglecting the Lagrangian density:[9,18,19,24]

$$\nabla^2 p - \frac{1}{c_0^2}\frac{\partial^2 p}{\partial t^2} = -\frac{\delta}{c_0^2}\nabla^2\frac{\partial p}{\partial t} - \frac{\beta}{\rho_0 c_0^4}\frac{\partial^2 p^2}{\partial t^2}. \tag{4}$$

In the inverse-law far field, the audio sound pressure amplitude is inversely proportional to the propagating distance so that the solution of the audio sound has the simplest form.

A. Near field

To solve Eq. (2) accurately and efficiently, its equivalent form, i.e. the Kuznetsov equation, is introduced in terms of the velocity potential Φ such that $\mathbf{v} = \nabla\Phi$,[18,19]

$$\nabla^2\Phi - \frac{1}{c_0^2}\frac{\partial^2\Phi}{\partial t^2} = -\frac{\delta}{c_0^2}\nabla^2\frac{\partial\Phi}{\partial t} + \frac{1}{c_0^2}\frac{\partial}{\partial t}\left[\left(\nabla\Phi\right)^2 + \frac{\beta-1}{c_0^2}\left(\frac{\partial\Phi}{\partial t}\right)^2\right]. \tag{5}$$

Because the ultrasound level generated by a PAL is limited, the nonlinearity is weak and the quasilinear approximation can be assumed.[1] After using the method of successive approximations,[28] Eq. (5) is decomposed into two coupled linear equations under the harmonic excitation

$$\begin{cases} \nabla^2\Phi_i + k_i^2\Phi_i = 0, \quad i = 1, 2 \\ \nabla^2\Phi_\mathrm{a} + k_\mathrm{a}^2\Phi_\mathrm{a} = q \end{cases}, \tag{6}$$

where the wavenumber $k_i = \omega_i/c_0 + \mathrm{j}\alpha_i$, α_i is the sound attenuation coefficient at frequency f_i, Φ_i is the velocity potential at frequency f_i, $i = 1$, 2, and "a", and q can be considered as the source density function of a volume virtual audio source occupying the whole space,[19]

$$q(\mathbf{r}) = -\frac{\mathrm{j}\omega_\mathrm{a}}{c_0^2}\left[(\beta-1)\frac{\omega_1\omega_2}{c_0^2}\Phi_1(\mathbf{r})\Phi_2^*(\mathbf{r}) + \mathbf{v}_1(\mathbf{r})\cdot\mathbf{v}_2^*(\mathbf{r})\right]. \tag{7}$$

Here, the superscript "*" denotes the complex conjugate, $\mathbf{v}_i = \nabla\Phi_i$ is the particle velocity for the ith ultrasonic wave, and $i = 1$ and 2.

The velocity potential of the ultrasound is calculated using the Rayleigh integral [Eq. (5.2.6) in Ref. 29]

$$\Phi_i(\mathbf{r}) = -\frac{v_{i,0}}{2\pi}\iint_S \frac{\mathrm{e}^{\mathrm{j}k_i d_\mathrm{s}}}{d_\mathrm{s}}\mathrm{d}x_\mathrm{s}\mathrm{d}y_\mathrm{s}, \tag{8}$$

where $d_\mathrm{s} = \sqrt{(x-x_\mathrm{s})^2 + (y-y_\mathrm{s})^2 + z^2}$ is the distance between the field point $\mathbf{r} = (x, y, z)$ and the source point $\mathbf{r}_{\mathrm{s}} = (x_{\mathrm{s}}, y_{\mathrm{s}}, z_{\mathrm{s}})$ with $z_{\mathrm{s}} = 0$ on the transducer surface, and the origin of the rectangular coordinate system *Oxyz* is the center of the PAL with the z-axis perpendicular to the transducer surface S. The orthogonal components under the system *Oxyz* of the velocity of ultrasound can be obtained by,[19]

$$\begin{cases} v_{i,x}(\mathbf{r}) = \dfrac{\partial \Phi_i(\mathbf{r})}{\partial x} = \dfrac{v_{i,0}}{2\pi} \iint_S (x - x_{\mathrm{s}})(1 - \mathrm{j}k_i d_{\mathrm{s}}) \dfrac{\mathrm{e}^{-\mathrm{j}k_i d_{\mathrm{s}}}}{d_{\mathrm{s}}^3} \mathrm{d}x_{\mathrm{s}} \mathrm{d}y_{\mathrm{s}} \\ v_{i,y}(\mathbf{r}) = \dfrac{\partial \Phi_i(\mathbf{r})}{\partial y} = \dfrac{v_{i,0}}{2\pi} \iint_S (y - y_{\mathrm{s}})(1 - \mathrm{j}k_i d_{\mathrm{s}}) \dfrac{\mathrm{e}^{-\mathrm{j}k_i d_{\mathrm{s}}}}{d_{\mathrm{s}}^3} \mathrm{d}x_{\mathrm{s}} \mathrm{d}y_{\mathrm{s}} \\ v_{i,z}(\mathbf{r}) = \dfrac{\partial \Phi_i(\mathbf{r})}{\partial z} = \dfrac{v_{i,0}}{2\pi} \iint_S z(1 - \mathrm{i}k_i d_{\mathrm{s}}) \dfrac{\mathrm{e}^{-\mathrm{j}k_i d_{\mathrm{s}}}}{d_{\mathrm{s}}^3} \mathrm{d}x_{\mathrm{s}} \mathrm{d}y_{\mathrm{s}} \end{cases} . \tag{9}$$

The source density function of the virtual audio source is obtained from Eqs. (7) to (9), and the velocity potential of audio sounds is an integral over the space, so that

$$\Phi_{\mathrm{a}}(\mathbf{r}) = -\frac{1}{4\pi} \int_{-\infty}^{\infty} \int_{-\infty}^{\infty} \int_{-\infty}^{\infty} q(\mathbf{r}_{\mathrm{v}}) \frac{\mathrm{e}^{\mathrm{j}k_{\mathrm{a}} d_{\mathrm{v}}}}{d_{\mathrm{v}}} \mathrm{d}x_{\mathrm{v}} \mathrm{d}y_{\mathrm{v}} \mathrm{d}z_{\mathrm{v}} , \tag{10}$$

where $d_{\mathrm{v}} = \sqrt{(x - x_{\mathrm{v}})^2 + (y - y_{\mathrm{v}})^2 + (z - z_{\mathrm{v}})^2}$ is the distance between the field point $\mathbf{r}$ and the virtual source point or its image at $\mathbf{r}_{\mathrm{v}} = (x_{\mathrm{v}}, y_{\mathrm{v}}, z_{\mathrm{v}})$.[21] The sound pressure of audio sounds can be obtained using its second-order relationship with the velocity potential as,[19]

$$p_{\mathrm{a}}(\mathbf{r}) = \mathrm{j}\omega_{\mathrm{a}} \rho_0 \Phi_{\mathrm{a}}(\mathbf{r}) - \frac{\rho_0}{2} \mathbf{v}_1(\mathbf{r}) \cdot \mathbf{v}_2^*(\mathbf{r}) + \frac{\rho_0 \omega_1 \omega_2}{2c_0^2} \Phi_1(\mathbf{r}) \Phi_2^*(\mathbf{r}) . \tag{11}$$

Equation (11) is the exact solution of the Kuznetsov equation under the quasilinear approximation, but is difficult to compute numerically due to the five-fold integral that arises after substituting Eqs. (7) to (10) into this equation. The well-known Gaussian beam expansion method cannot be used here to simplify the calculations because significant errors are introduced in the near field no matter how many Gaussian beams are used.[30,31] In the following paragraphs, the five-fold integral in Eq. (11) is simplified based on a spherical harmonic expansion method that removes the need for additional approximations.

To simplify the sound pressure of ultrasound, a spherical coordinate system (r, θ, φ) is adopted, where r, θ, and φ are the radial distance, polar angle, and azimuthal angle, respectively. The Green's function in free field, i.e., $\mathrm{e}^{\mathrm{j}k_i d_\mathrm{s}}/(4\pi d_\mathrm{s})$ in Eq. (8), can be expanded in spherical coordinates as a summation of spherical harmonic terms. After utilizing the orthogonal properties of Legendre polynomials and trigonometric functions, the velocity potential can be simplified as[21]

$$\Phi_i(\mathbf{r}) = \frac{-\mathrm{j}v_{i,0}}{k_i}\sum_{n=0}^{\infty} C_n \mathrm{P}_{2n}(\cos\theta) R_{i,n}(r), \quad i = 1,2, \tag{12}$$

where the coefficient and the radial component of ultrasound are

$$C_n = (-1)^n (4n+1)\frac{\Gamma(n+\frac{1}{2})}{\sqrt{\pi}\,\Gamma(n+1)}, \tag{13}$$

$$R_{i,n}(r) = \int_0^a \mathrm{j}_{2n}(k_i r_{\mathrm{s},<})\mathrm{h}_{2n}(k_i r_{\mathrm{s},>}) k_i^2 r_\mathrm{s} \mathrm{d}r_\mathrm{s}, \tag{14}$$

respectively. In addition, $\Gamma(\cdot)$ is the Gamma function, $\mathrm{j}_{2n}(\cdot)$ is the spherical Bessel function, $\mathrm{h}_{2n}(\cdot)$ is the spherical Hankel function of the first kind, $\mathrm{P}_{2n}(\cdot)$ is the Legendre polynomial, $r_{\mathrm{s},>} = \max(r, r_\mathrm{s})$, and $r_{\mathrm{s},<} = \min(r, r_\mathrm{s})$.

The components of the acoustic particle velocity under the spherical coordinate system can be obtained directly from Eq. (12), to give

$$\begin{cases} v_{i,r}(\mathbf{r}) = \dfrac{\partial \Phi_i(\mathbf{r})}{\partial r} = -\mathrm{j}v_{i,0}\displaystyle\sum_{n=0}^{\infty} C_n \mathrm{P}_{2n}(\cos\theta)\frac{\mathrm{d}\,R_{i,n}(r)}{\mathrm{d}(k_i r)} \\ v_{i,\theta}(\mathbf{r}) = \dfrac{1}{r}\dfrac{\partial \Phi_i(\mathbf{r})}{\partial \theta} = -\mathrm{j}v_{i,0}\displaystyle\sum_{n=0}^{\infty} C_n \frac{\mathrm{d}\,\mathrm{P}_{2n}(\cos\theta)}{\mathrm{d}\theta}\frac{R_{i,n}(r)}{k_i r} \\ v_{i,\varphi}(\mathbf{r}) = \dfrac{1}{r\sin\theta}\dfrac{\partial \Phi_i(\mathbf{r})}{\partial \varphi} = 0 \end{cases}. \tag{15}$$

Equations (12) and (15) represent rigorous transformations of the Rayleigh integrals in Eqs. (8) and (9), and these have been shown to facilitate fast computation times.[32] The integral in Eq. (14) can be calculated either by the numerical integration[21] or generalized hypergeometric functions.[32,33]

The source density function in Eq. (7) can be rewritten as

$$q(\mathbf{r}) = -\frac{\mathrm{j}\omega_{\mathrm{a}}}{c_0^2}\left[(\beta-1)\frac{\omega_1\omega_2}{c_0^2}\Phi_1(\mathbf{r})\Phi_2^*(\mathbf{r}) + v_{1,r}(\mathbf{r})v_{2,r}^*(\mathbf{r}) + v_{1,\theta}(\mathbf{r})v_{2,\theta}^*(\mathbf{r})\right]. \tag{16}$$

After substituting the spherical expansion expressions from Eqs. (12) and (15) into Eqs. (10) and (16), the velocity potential of audio sounds can be written as

$$\Phi_{\mathrm{a}}(\mathbf{r}) = \Phi_{\mathrm{p}}(\mathbf{r}) + \Phi_r(\mathbf{r}) + \Phi_\theta(\mathbf{r}), \tag{17}$$

where the three components on the right-hand side of the equation are the contributions from the corresponding components in Eq. (16), and they are (see Appendix for derivations)

$$\Phi_{\mathrm{p}}(\mathbf{r}) = -(\beta-1)\frac{v_{1,0}v_{2,0}^*}{\omega_{\mathrm{a}}}\sum_{l,m,n=0}^{\infty} C_l C_m W_{lmn} \mathrm{P}_{2n}(\cos\theta) F_{\mathrm{p}}(r), \tag{18}$$

$$\Phi_r(\mathbf{r}) = -\frac{v_{1,0}v_{2,0}^*}{\omega_{\mathrm{a}}}\sum_{l,m,n=0}^{\infty} C_l C_m W_{lmn} \mathrm{P}_{2n}(\cos\theta) F_r(r), \tag{19}$$

$$\Phi_\theta(\mathbf{r}) = -\frac{v_{1,0}v_{2,0}^*}{\omega_{\mathrm{a}}}\sum_{l,m,n=0}^{\infty} C_l C_m W_{lmn}[l(2l+1)+m(2m+1)-n(2n+1)] \mathrm{P}_{2n}(\cos\theta) F_\theta(r), \tag{20}$$

where the triple summation $\sum_{l,m,n=0}^{\infty} = \sum_{l=0}^{\infty}\sum_{m=0}^{\infty}\sum_{n=0}^{\infty}$ and the coefficient

$$W_{lmn} = (4n+1)\begin{pmatrix} 2l & 2m & 2n \\ 0 & 0 & 0 \end{pmatrix}^2, \tag{21}$$

which contains the Wigner 3j symbol, and this can be calculated using a closed-form formula [see Eq. (C.23) in Ref. 34, or Eq. (20) in Ref. 21]. The triangular inequality should also be satisfied, so that $|l-m| \le n \le l+m$. The radial components of audio sounds $F_{\mathrm{p}}(r)$, $F_r(r)$, and $F_\theta(r)$ are then given as

$$F_{\mathrm{p}}(r) = \int_0^{\infty} R_{1,l}(r_{\mathrm{v}}) R_{2,m}^*(r_{\mathrm{v}}) \mathrm{h}_{2n}(k_{\mathrm{a}} r_{\mathrm{v},>}) \mathrm{j}_{2n}(k_{\mathrm{a}} r_{\mathrm{v},<}) k_{\mathrm{a}}^3 r_{\mathrm{v}}^2 \mathrm{d}r_{\mathrm{v}}, \tag{22}$$

$$F_r(r) = \int_0^{\infty} \frac{\mathrm{d}R_{1,l}(r_{\mathrm{v}})}{\mathrm{d}(k_1 r_{\mathrm{v}})} \frac{\mathrm{d}R_{2,m}^*(r_{\mathrm{v}})}{\mathrm{d}(k_2^* r_{\mathrm{v}})} \mathrm{h}_{2n}(k_{\mathrm{a}} r_{\mathrm{v},>}) \mathrm{j}_{2n}(k_{\mathrm{a}} r_{\mathrm{v},<}) k_{\mathrm{a}}^3 r_{\mathrm{v}}^2 \mathrm{d}r_{\mathrm{v}}, \tag{23}$$

$$\text{and} \quad F_\theta(r) = \int_0^\infty R_{1,l}(r_\mathrm{v}) R_{2,m}^*(r_\mathrm{v}) \mathrm{h}_{2n}(k_\mathrm{a} r_{\mathrm{v},>}) \mathrm{j}_{2n}(k_\mathrm{a} r_{\mathrm{v},<}) \frac{k_\mathrm{a}^3}{k_1 k_2^*} \mathrm{d}r_\mathrm{v} \,, \tag{24}$$

respectively, where $r_{\mathrm{v},<} = \min(r, r_\mathrm{v})$, $r_{\mathrm{v},>} = \max(r, r_\mathrm{v})$, and r_v is the radial coordinate of the virtual source point $\mathbf{r}_\mathrm{v}$.

Equations (17) to (24) are the main results of this section. The audio sound pressure can be obtained by substituting Eqs. (12), (15), and (17) into Eq. (11). Equation (17) is solved by the Kuznetsov equation with the quasilinear assumption and this is exact over the entire field. Because no additional assumptions are made in the derivation, it is equivalent to the original solution to Eq. (10) that contains five-fold integrals. The proposed expressions in Eqs. (18) to (20) can be calculated more efficiently for 3 reasons: (i) it is a series with a three-fold summation consisting of uncoupled spherical angular and radial components; (ii) the radial components $F_\mathrm{p}(r)$, $F_r(r)$, and $F_\theta(r)$ can be transformed into a rapidly converged integral using the property of spherical Bessel functions (see Ref. 21 for details); and, (iii) a number of the terms do not need to be calculated because many values of the Wigner 3j symbol are zero due to the restrictions of the triangular inequality.

B. Westervelt far field

In the Westervelt far field, the Westervelt equation, Eq. (4), is used to calculate the audio sound pressure. The source density function of the virtual sound source, Eq. (7), and the relationship between the sound pressure and velocity potential of audio sounds, Eq. (11), are then simplified as

$$q(\mathbf{r}) = -\frac{\mathrm{j}\beta\omega_\mathrm{a}\omega_1\omega_2}{c_0^4} \Phi_1(\mathbf{r}) \Phi_2^*(\mathbf{r}) \,, \tag{25}$$

$$\text{and} \quad p_\mathrm{a}(\mathbf{r}) = \mathrm{j}\omega_\mathrm{a}\rho_0 \Phi_\mathrm{a}(\mathbf{r}) \,, \tag{26}$$

respectively. In this case, the audio sound pressure is reduced to

$$p_\mathrm{a}(\mathbf{r}) = -\mathrm{i}\beta\rho_0 v_{1,0} v_{2,0}^* \sum_{l,m,n=0}^{\infty} C_l C_m W_{lmn} \mathrm{P}_{2n}(\cos\theta) F_\mathrm{p}(r) \,, \tag{27}$$

which is the same as Eq. (21) in Ref. 21.

C. Inverse-law far field

Asymptotic formula for spherical Hankel functions at $k_\mathrm{a}r \to \infty$ yields

$$\mathrm{h}_{2n}(k_\mathrm{a}r) \sim (-1)^n \frac{\mathrm{e}^{\mathrm{j}k_\mathrm{a}r}}{\mathrm{j}k_\mathrm{a}r}. \tag{28}$$

And the radial component in Eq. (27), $F_\mathrm{p}(r)$, can be simplified as

$$F_\mathrm{p}(r) = (-1)^n \frac{\mathrm{e}^{\mathrm{j}k_\mathrm{a}r}}{\mathrm{j}k_\mathrm{a}r} \int_0^\infty R_{1,l}(r_\mathrm{v}) R_{2,m}^*(r_\mathrm{v}) \mathrm{j}_{2n}(k_\mathrm{a}r_\mathrm{v}) k_\mathrm{a}^3 r_\mathrm{v}^2 \mathrm{d}r_\mathrm{v}. \tag{29}$$

By substituting Eq. (29) into Eq. (27), it is clear that the audio sound pressure amplitude is inversely proportional to the propagating distance, r, so that the audio sound in the inverse-law far field is obtained. It is noteworthy that the solution obtained here is more accurate than existing ones, such as Refs. 9 and 14, because the complex nonlinear interactions in the near field of the PAL are more accurately captured.

D. Consistency of governing equations and solutions

To make the methods easy to follow, the relationships among the important governing equations and the solutions in the near field, the Westervelt far field, and the inverse-law far field are presented in Fig. 1. The Lighthill equation is derived from conservation of mass and conservation of momentum without approximations. The equation of state is then used to obtain a second-order nonlinear wave equation, Eq. (2), where the terms of cubic and higher order in the acoustic variables are ignored.[18] The Kuznetsov equation, Eq. (5), is equivalent to the second-order nonlinear wave equation but is expressed in terms of the velocity potential instead of the sound pressure.[19] The near field solution in Eq. (11), is obtained from the Kuznetsov equation under a quasilinear assumption.

By neglecting the local effects (characterized by the Lagrangian density) in the second-order nonlinear wave equation, the Westervelt equation, Eq. (4), is obtained, and the quasilinear solution of this equation is reported in Eq. (27) after substituting Eq. (22) into it. If the asymptotic limit, Eq. (28), is employed for the spherical Hankel functions, the inverse-law far field solution is obtained as Eq. (27) after substituting Eq. (29) into it. It is also noted that the KZK equation is a paraxial approximation of the Westervelt equation and the Burgers equation is the one-dimensional form of the KZK equation without accounting the diffraction effects.[24]

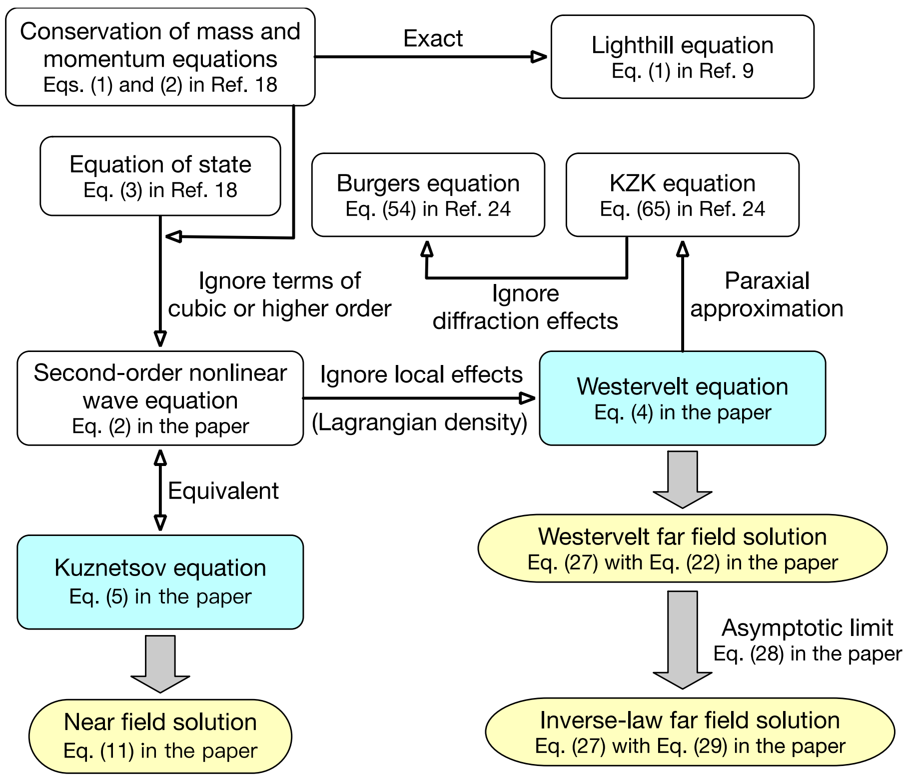

Fig. 1. (Color online) Relationships among the governing equations and the solutions in different fields presented in this paper.

III. SIMULATIONS AND DISCUSSIONS

Numerical simulations are conducted here using MATLAB R2018a. The sound attenuation coefficients of the ultrasound and audio sounds in air are calculated according to ISO 9613-1 with the relative humidity 60% and temperature 25°C.[35] The vibration velocity amplitude at two ultrasonic frequencies are $v_{1,0} = v_{2,0} = 0.1$ m/s. Because there are two ultrasound frequencies, the average of them, $f_u = (f_1 + f_2)/2$, is used in the following text for clarity. The wavenumber at f_u is therefore denoted by k_u. The reference quantity for the sound pressure level (SPL) used in the following text is 20μ Pa. The results calculated by the quasilinear solution based on Kuznetsov equation [Eq. (2)], Westervelt equation [Eq. (4)], and the inverse-law property [Eq. (29)] are denoted by "Kuznetsov", "Westervelt", and "Inverse-law", respectively. As shown in the spherical expansions in Eqs. (18) to (20) and (27), the audio sound pressure and velocity potential are obtained by using the three-fold summation series with respect to l, m, and n, with the truncated term being set as N for all l, m, and n for simplicity.

A. Validation of the proposed calculation method

To illustrate the accuracy and efficiency of the proposed method in Sec. II.A, the parameters in Ref. 19 are used and also listed in Table I. Figure 2 shows the audio sound pressure level (SPL) as a function of the truncated term N at several typical field points when $y = 0$. It is clear that all the curves converge with sufficient terms. The truncated error is less than 0.1 dB when the truncated term N is larger than 10.

Table I. The parameters used for validating the proposed method in Sec. II.A.

Item	Value
Average ultrasound frequency	$f_u = 39.5$ kHz
Audio frequency	$f_a = 1$ kHz
Sound attenuation coefficients	$\alpha_1 = \alpha_2 = 2.8 \times 10^{-2}$ Np/m $\alpha_a = 6.9 \times 10^{-4}$ Np/m
Transducer surface radius	$a = 0.02$ m
Helmholtz number	$k_u a = 14.7$
Rayleigh distance	0.146 m

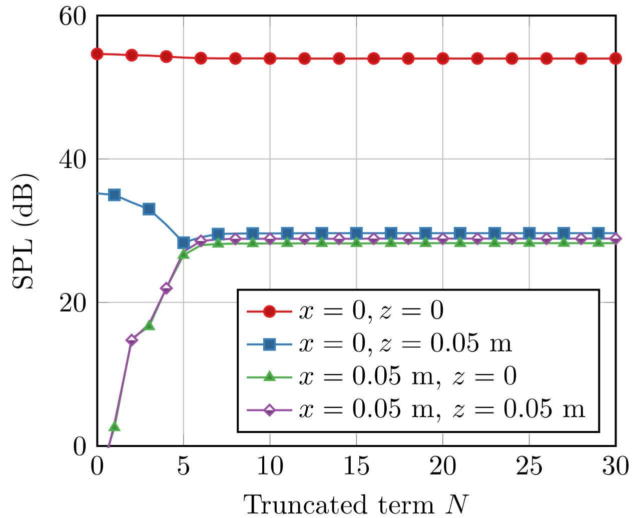

Fig. 2. (Color online) Convergence of the audio sound SPL as a function of the truncated term N at several typical field points when $y = 0$, where the parameters in Table I are used.

For comparison, the direct integration of Eq. (10) is performed (denoted by "direct method"), where the 1/3 Simpson rule is used for numerical integrations. The integrated coordinates are evenly discretized, and the field coordinate is set as the middle point between adjacent integrated coordinates to avoid singularities of Green's functions. The infinitely large integral domain is reduced to a cylindrical column centered along the axis of the PAL with a radius of 1.5 m and a length of 3 m to cover the major energy of ultrasonic beams. Figure 3 shows the audio SPL as a function of the propagating distance in different directions at 1 kHz, where the results obtained by the proposed method are same as that from the direct method. But the proposed method is faster than the direct method to calculate the audio sound in different directions because the polar angle coordinate, θ, of the field point is uncoupled in the expression. For example, the radial components in Eqs. (22) to (24) need to be calculated only once when obtaining the 3 curves in Fig. 3.

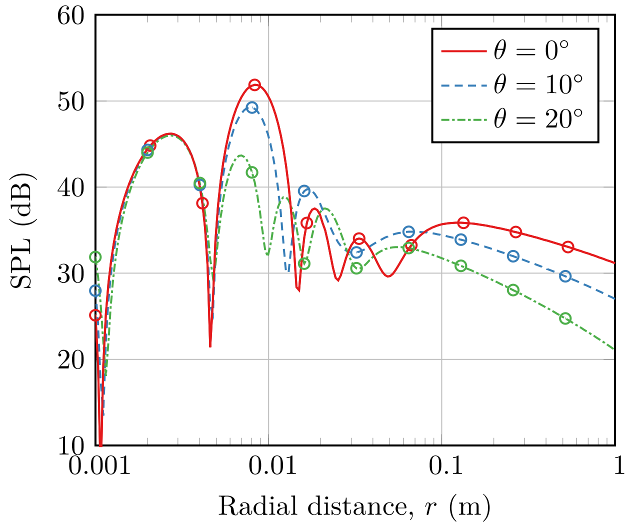

Fig. 3. (Color online) The audio SPL as a function of the propagating distance in different directions at 1 kHz, where the circles are that obtained by using the direct method.

Table II lists the computation time of the proposed and direct methods at 3 typical field points. The precision criterion is used to identify the difference between the SPL calculated with the two methods to be less than 0.05 dB. The calculation was conducted on a personal computer with 2.5 GHz main frequency and 16 GB random access memory. Table II demonstrates that the computation time of the proposed method remains similar for all the cases, but is at least 100 times faster than the direct method. The reason for the computation saving is that the direct method has to calculate the sound pressure of the ultrasound at many virtual source points and then integrate over a large space, but this is not required in the proposed new method.

B. Regions of the audio sound field of the PAL

Figure **4** shows the audio SPL as a function of the propagating distance at 1 kHz calculated with different methods, where the transducer radius is 0.05 m and the average ultrasound frequency is 40 kHz. Here, the results obtained by the 3 methods are different, from which the audio sound field is proposed to be divided into 3 regions: near field, Westervelt far field, and inverse-law far field.

Table II. Comparison of the computation time of the proposed and direct methods.

Field points	Calculation time (s)	
	Proposed method	Direct method
$x = y = 0$ and $z = 0.05$ m (On-axis)	0.59	75.2
$x = 0.05$ m, $y = 0$, and $z = 0.05$ m (Off-axis)	0.56	82.5
$x = y = z = 0$ (Close to the PAL)	0.64	354.6

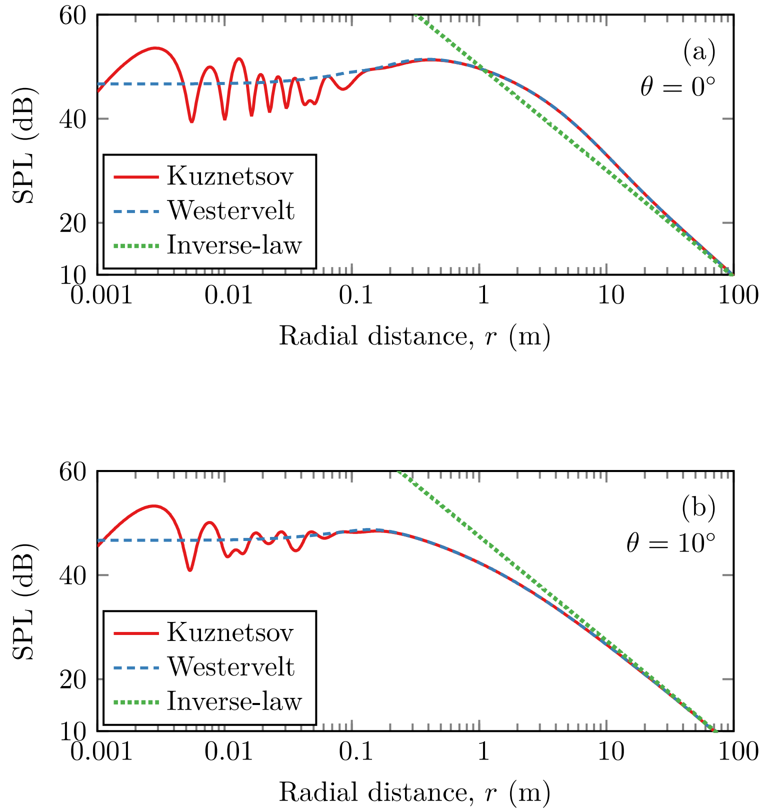

FIG. 4. (Color online) The audio SPL as a function of the propagating distance at 1 kHz calculated with different methods: (a) on the radiation axis (0°), and (b) in the direction 10°, where the transducer radius is 0.05 m and the average ultrasound frequency is 40 kHz.

In the near field, the audio SPL is complicated and local maxima and minima take place due to strong local effects characterized by the ultrasonic Lagrangian density, so here the Kuznetsov equation must be used. When the radial distance is larger than 0.42 m and 0.19 m in Figs. 4(a) and (b), respectively, the difference between the curves denoted by "Kuznetsov" and "Westervelt" is less than 0.1 dB, and so the Westervelt equation may be used to predict the audio sound in the Westervelt far field. The inverse-law far field is the region where the radial distance is larger than 28.7 m and 7.3 m in Figs. 4(a) and (b), respectively, and the difference between the curves denoted by "Westervelt" and "Inverse-law" is less than 1 dB. The transition distances among these regions are the largest on the radiation axis, so only the sounds on the radiation axis are considered in the following simulations for simplicity.

C. The transition distance from the near field to the Westervelt far field

Figure 5 shows the audio SPL at 1 kHz and the ultrasound field at 40 kHz on the radiation axis as a function of the propagating distance, where the transducer radius is 0.05 m. The ultrasound pressure is calculated with the closed-form formula [Eq. (5.7.3) in Ref. 29]

$$p_{\mathrm{u}}(z) = -2\mathrm{j}\rho_0 c_0 v_0 \mathrm{e}^{\mathrm{j}\frac{k_{\mathrm{u}}a}{2}\left(\sqrt{1+\frac{z^2}{a^2}}+\frac{z}{a}\right)} \sin\left[\frac{k_{\mathrm{u}}a}{2}\left(\sqrt{1+\frac{z^2}{a^2}}-\frac{z}{a}\right)\right], \tag{30}$$

where k_{u} is the wavenumber at the average ultrasound frequency f_{u}, and v_0 is the vibration velocity amplitude. The ultrasonic Lagrangian density is approximated by neglecting the particle velocity components in the x and y directions in Eq. (3) as

$$L_{\mathrm{u}}(z) = \frac{1}{2}\rho_0 v_{\mathrm{u},z}^2(z) - \frac{p_{\mathrm{u}}^2(z)}{2\rho_0 c_0^2}, \tag{31}$$

where $v_{\mathrm{u},z}$ is the particle velocity component in z direction and can be obtained by the relation $v_{\mathrm{u},z} = (\mathrm{j}k_{\mathrm{u}}\rho_0 c_0)^{-1}\partial p_{\mathrm{u}}/\partial z$, and Eq. (30) as

$$v_{\mathrm{u},z}(z) = v_0 \mathrm{e}^{\mathrm{j}k_{\mathrm{u}}z} - v_0\frac{z}{a}\left(1+\frac{z^2}{a^2}\right)^{-1/2} \mathrm{e}^{\mathrm{j}k_{\mathrm{u}}a\sqrt{1+\frac{z^2}{a^2}}}. \tag{32}$$

The obtained ultrasound pressure and Lagrangian density on the radiation axis are then normalized by $2\rho_0 c_0 v_0$ and $2\rho_0 v_0$, respectively, and are shown in Fig. 5(b).

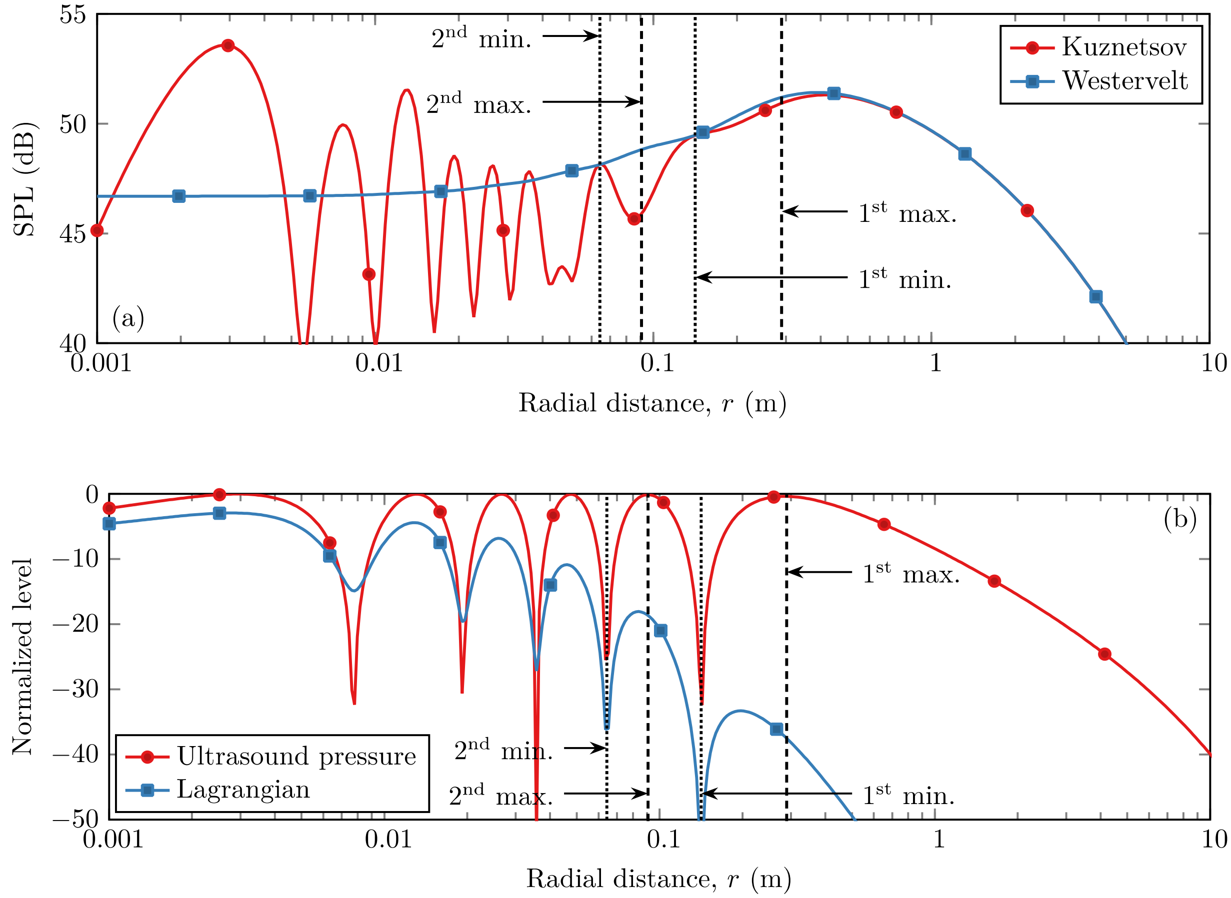

FIG. 5. (Color online) (a) The audio SPL at 1 kHz and (b) the level of normalized ultrasound pressure and Lagrangian density at the average ultrasound frequency 40 kHz, as a function of the propagating distance on the radiation axis, where the transducer radius is 0.05 m.

The ultrasound pressure amplitude has several local minima and maxima in the near field. From Eq. (30), the radial distance at the local minima can be obtained by [Eq. (5.7.4) in Ref. 29]

$$r_{\min}(n) = \left[\left(\frac{a}{\lambda_{\mathrm{u}}}\right)^2 - n^2\right]\frac{\lambda_{\mathrm{u}}}{2n},\ n = 1, 2, \ldots, \lfloor a/\lambda_{\mathrm{u}} \rfloor, \tag{33}$$

where λ_{u} is the wavelength at the average ultrasound frequency f_{u} and $\lfloor \cdot \rfloor$ rounds down the quantity inside. Similarly, the radial distance at the local maxima can be obtained by

$$r_{\max}(n)=\left[\left(\frac{a}{\lambda_{\mathrm{u}}}\right)^2-\left(\frac{2n-1}{2}\right)^2\right]\frac{\lambda_{\mathrm{u}}}{2n-1},\ n=1,2,\ldots,\lfloor a/\lambda_{\mathrm{u}}+1/2\rfloor. \tag{34}$$

The first two (n = 1 and 2) local minima and maxima are plotted in Fig. 5. It appears that the locations of local maxima and minima of ultrasonic Lagrangian density are close to that of the ultrasound pressure.

The ultrasonic Lagrangian density is non-cumulative as the propagation of the ultrasound beams.[18] In the near field, where the field point is close to a PAL, the ultrasonic Lagrangian density fluctuates significantly, and the audio sound calculated with the Kuznetsov equation in Fig. 5(a) is complicated which means that the results obtained with the Westervelt equation are inaccurate. Figure 5(b) shows that the ultrasonic Lagrangian density is small when the radial distance is larger than the first local maximum (0.29 m in this case), and the results calculated with the Westervelt equation in Fig. 5(a) are also accurate.

The transition from the near field to the Westervelt far field is affected by the local minima and maxima of the ultrasound pressure amplitude. As shown in in Fig. 5(b), at the first two local minima, the normalized Lagrangian density is more than 30 dB lower than that near the PAL, so it can be neglected in the calculation of audio sounds and the results obtained by the Kuznetsov and Westervelt equations are almost the same, as shown in Fig. 5(a). At the distance of the first two local maxima, the Lagrangian density amplitude is near its local maxima, so its effects are prominent and the difference between the results obtained by the Kuznetsov and Westervelt equations is large. The difference decreases as the ordinal number of the local maximum decreases. For example, the difference is 3.0 dB at the second local maximum (0.09 m) and it decreases to 0.3 dB at the first local maximum (0.29 m).

Figure 6 shows the difference of the audio SPL calculated with the Kuznetsov and Westervelt equations as a function of the propagating distance on the radiation axis, with different transducer radii at different ultrasound frequencies for an audio frequency of 1 kHz. The radial distance to the first maximum of the ultrasound pressure amplitude is listed in Table

III and calculated by setting $n = 1$ in Eq. (34), so that

$$r_{\max}(1) = \frac{a^2}{\lambda_u} - \frac{\lambda_u}{4}. \tag{35}$$

At large radial distances, the audio SPL difference approaches 0 dB indicating the accuracy of using the Westervelt equation. At small radial distances, the number of local minima and maxima increases as the transducer radius and ultrasound frequency increases, as predicted from Eqs. (33) and (34).

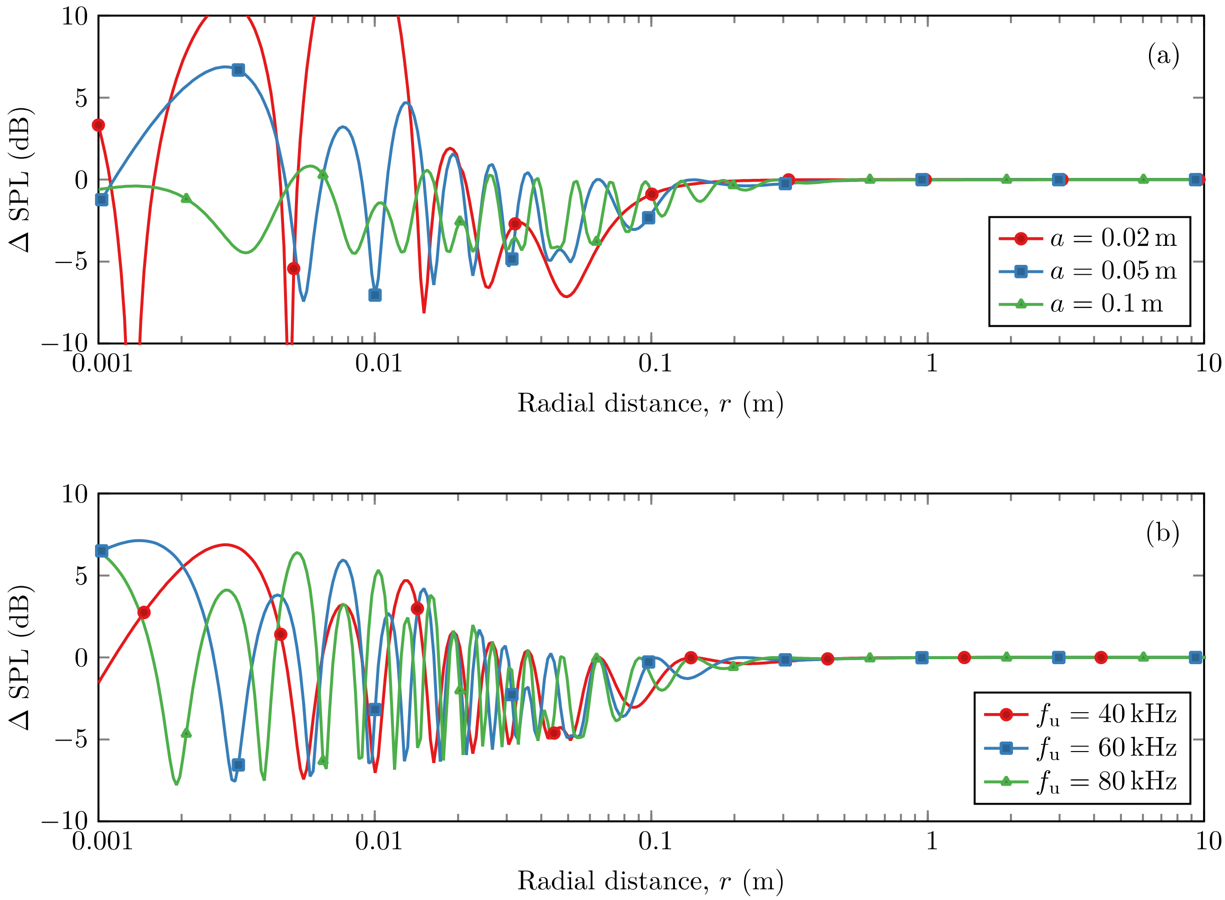

FIG. 6. (Color online) The audio SPL difference calculated with the Kuznetsov and Westervelt equations as a function of the propagating distance on the radiation axis (a) with different transducer radii when the average ultrasound frequency is 40 kHz, and (b) at different average ultrasound frequencies when the transducer radius is 0.05 m, where the audio frequency is 1

kHz.

Table III. The first maxima of the ultrasound pressure amplitude and the transition distances from the near field to the Westervelt far field for several sets of parameters.

Transducer radius (m)	Ultrasound frequency f_u (kHz)	First maximum $r_{max}(1)$ (m)	Transition distance from the near field to the Westervelt far field (m)
0.02	40	0.04	0.04 ($n_0 = 1$)
0.05	40	0.29	0.29 ($n_0 = 1$)
0.1	40	1.16	0.38 ($n_0 = 2$)
0.15	40	2.62	0.51 ($n_0 = 3$)
0.2	40	4.67	0.65 ($n_0 = 4$)
0.25	40	7.29	0.79 ($n_0 = 5$)
0.05	60	0.44	0.44 ($n_0 = 1$)
0.05	80	0.58	0.19 ($n_0 = 2$)
0.05	100	0.73	0.24 ($n_0 = 2$)
0.05	120	0.87	0.17 ($n_0 = 3$)

The distance at the n-th local maximum of the ultrasound pressure amplitude increases as the transducer radius and ultrasound frequency increase, where n is any positive integer number restricted by the condition in Eq. (34). The audio SPL difference at the location of the corresponding local maximum decreases if the transducer radius and ultrasound frequency increase. This is because the ultrasound beam is more collimated when the transducer radius and the ultrasound frequency are larger. The ultrasound beams can also be approximated by plane waves when they are highly collimated. In this case, the ultrasonic Lagrangian density approaches zero after substituting the plane wave condition $|p_u| = \rho_0 c_0 |v_{u,z}|$ into Eq. (31), which means the local effects are negligible and the Westervelt equation is accurate. Therefore, the magnitude of the audio SPL difference can be determined by how much the ultrasound beams behave like plane waves, which is measured by defining an error function as

$$\varepsilon(z) = \left[1 - \frac{\rho_0 c_0 |v_{\mathrm{u},z}(z)|}{|p_\mathrm{u}(z)|}\right] \times 100\% . \tag{36}$$

If the error function is small, the ultrasound beams are more collimated and the effects of the ultrasonic Lagrangian density would also be small.

Because the audio SPL difference calculated with the two equations is large at points near the local maxima of the ultrasound pressure amplitude, the transition distance from the near field to the Westervelt far field can be defined as the distance at the n_0-th local maximum of the ultrasound pressure amplitude, such that the error function at this point is less than a threshold $\varepsilon_0 > 0$. To obtain n_0, the following condition should be satisfied as

$$\varepsilon[r_{\max}(n_0)] \le \varepsilon_0 . \tag{37}$$

Substituting Eqs. (34) and (36) into Eq. (37), n_0 is obtained by

$$n_0 = \max\left(1,\ \left\lfloor \frac{a}{\lambda_\mathrm{u}} \frac{1}{\sqrt{\varepsilon_0^{-1} - 1}} + \frac{1}{2} \right\rfloor\right), \tag{38}$$

where max(1, ·) is used to ensure n_0 is at least 1. The choice of a smaller threshold for ε_0 leads to higher precision when using the Westervelt equation to predict audio sounds in the Westervelt far field, region $r \ge r_{\max}(n_0)$. The transition distance at several sets of parameters are listed in Table III when ε_0 = 2.5%, and the numerical simulations show the error using the Westervelt equation is less than 0.6 dB under this condition.

Figure 7 shows the audio SPL difference at different audio frequencies when the transducer radius is 0.05 m, and the average ultrasound frequency is 40 kHz. At high audio frequencies, the audio SPL difference is small at small radial distances. This is because the audio SPL calculated with the Westervelt equation increases by about 12 dB when the audio frequency is doubled, but the amplitude of the ultrasonic Lagrangian density changes little at different audio frequencies, so its effect on the audio SPL is relatively small at high audio frequencies. The locations of local minima and maxima in the ultrasound pressure amplitude do not change at different audio frequencies, so the transition distance from the near field to the Westervelt far field does not vary with the audio frequency.

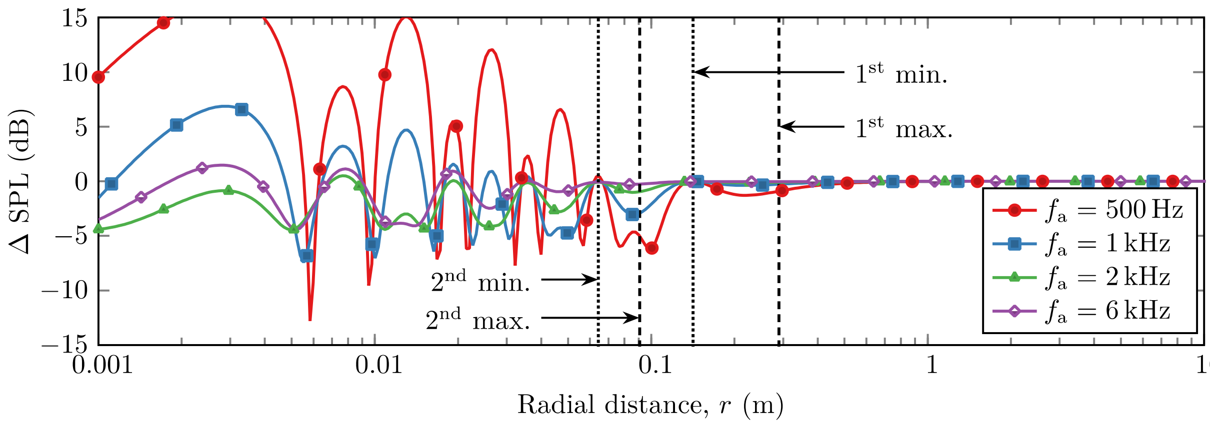

FIG. 7. (Color online) The audio SPL difference calculated with the Kuznetsov and Westervelt equations as a function of the propagating distance on the radiation axis at different audio frequencies (transducer radius is 0.05 m and the average ultrasound frequency is 40 kHz).

In this section, the formula of the transition distance from the near field to the Westervelt far field is derived based on the transducer with a uniform velocity profile. For other velocity profiles such as parabolic and quartic ones,[19] an appropriate formula can be obtained using a method similar to the one described above. For a specific velocity profile, the key step is to find the location of the local maxima of ultrasound pressure amplitude on the transducer axis, where the Lagrangian density amplitude is large and the local effects are significant.

D. The transition distance from the Westervelt far field to the inverse-law far field

Figure 8 shows the difference between the audio SPL calculated with the Westervelt equation and the inverse-law property, as a function of the propagating distance on the radiation axis with different transducer radii at different ultrasound and audio frequencies. This difference increases as the radial distance increases, and then decreases and approaches 0 dB at large radial distances, where the prediction based on the inverse-law property is accurate. Taking 1 dB as the error bound, this defines the region where the audio SPL difference is less than 1 dB to be the inverse-law far field. Table IV lists the transition distances from the Westervelt far field to the inverse-law far field for the parameters used in Fig. 8.

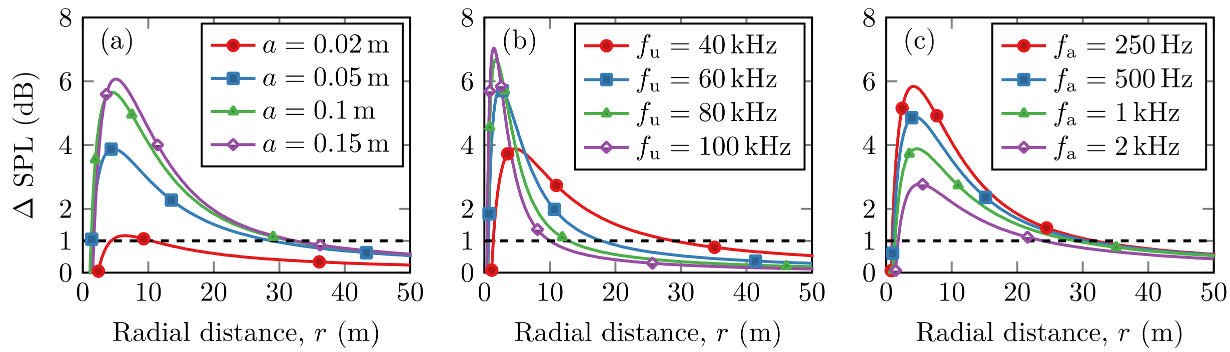

FIG. 8. (Color online) The audio SPL difference calculated with the Westervelt equation and the inverse-law property as a function of the propagating distance on the radiation axis (a) with different transducer radii when the average ultrasound frequency is 40 kHz and the audio frequency is 1 kHz, (b) at different average ultrasound frequencies when the transducer radius is 0.05 m and the audio frequency is 1 kHz, and (c) at different audio frequencies when the transducer radius is 0.05 m and the average ultrasound frequency is 40 kHz, where ΔSPL = 1 dB for the dashed lines.

Table IV. The transition distance from the Westervelt far field to the inverse-law far field for the parameters in Fig. 8.

Transducer radius a (m)	Ultrasound frequency f_u (kHz)	Audio frequency f_s (Hz)	Inverse-law transition distance (m) when ΔSPL < 1 dB
0.02	40	1000	10.6
0.05	40	1000	29.1
0.1	40	1000	31.8
0.15	40	1000	33.0
0.05	60	1000	17.8
0.05	80	1000	12.8

0.05	100	1000	10.2
0.05	40	250	32.3
0.05	40	500	30.6
0.05	40	2000	23.9

Figure 8(a) shows that the transition distance increases as the transducer radius increases. For example, it increases from 10.6 m to 29.1 m as the transducer radius increases from 0.02 m to 0.05 m. This is because the effective virtual source containing the major ultrasonic energy becomes larger as the transducer radius increases. Figure 8(b) shows that the transition distance decreases as the ultrasound frequency increases. For example, it decreases from 29.1 m to 17.8 m when the ultrasound frequency increases from 40 kHz to 60 kHz. This is because the effective virtual source becomes smaller as the sound attenuation coefficient of ultrasound beams in air becomes larger. Although the transition distance decreases as the audio frequency increases Fig. 8(c), the effects are relatively small. For example, it decreases by only 1.5 m (4.9%) when the audio frequency increases from 500 Hz to 1 kHz.

The effects of the transducer radius, and the ultrasound and audio frequencies on the inverse-law transition distance, are more complicated than the one from the near field to the Westervelt far field. It seems that the ultrasound frequency is the most important parameter because the ultrasound attenuation coefficient in air changes significantly as the frequency and meteorological conditions change. Therefore, an empirical formula, for example $4/\alpha_u$, can be used to estimate the inverse-law far field transition distance, where α_u is the ultrasound attenuation coefficient in air at the average ultrasound frequency f_u. The physical meaning of this formula is that the ultrasound pressure amplitude at this location has been attenuated to 2% ($e^{-4} \approx 0.02$). However, the formula does not hold for the very small sound absorption coefficient.

IV. CONCLUSIONS

In this paper, the audio sound field generated by a PAL is proposed to be divided into three regions: near field, Westervelt far field, and inverse-law far field. In the near field, the local effects characterized by the ultrasonic Lagrangian density are strong so that the Kuznetsov equation should be used to predict the audio sound. An efficient method based on a spherical harmonic expansion is proposed to calculate the quasilinear solution without loss of accuracy for a circular PAL. In the Westervelt far field, the local effects are negligible due to their non-cumulative property so that the well-known Westervelt equation is accurate. In the inverse-law far field, the audio sound pressure amplitude is inversely proportional to the propagating distance so the solution of the audio sound has the simplest form. With the proposed classification and methods, appropriate prediction models at different approximation levels can be chosen for each region.

The simulation results show that the boundary between the near field and Westervelt far field is approximately $a^2/\lambda - \lambda/4$, where a is the PAL radius and λ is the ultrasonic wavelength. At large transducer radii and high ultrasound frequencies, the boundary becomes closer to the PAL and a closed-form formula is presented to modify this value. The transition distance from the Westervelt far field to the inverse-law far field is more complicated. The ultrasound frequency is found to be the most important parameter and the transition distance can be approximately estimated with the empirical formula $4/\alpha$, where α is the ultrasound attenuation coefficient in air at the ultrasound frequency. Future work is to study the audio sound field generated by a PAL phased array.

ACKNOWLEDGEMENTS

This research is supported under the Australian Research Council's Linkage Project funding scheme (LP160100616).

APPENDIX

Equations (18) and (19) can be obtained by substituting the spherical expansions of ultrasonic waves Eqs. (12) and (15) into Eqs. (16) and (10), which is similar to the method used in Ref. 21. Equation (20) can be obtained similarly but a special integral is occurred due to the derivatives of Legendre polynomials as shown in Eq. (15),

$$I(l,m,n)=\int_{-1}^{1}\frac{\mathrm{d}\,\mathrm{P}_{2l}(x)}{\mathrm{d}\,x}\frac{\mathrm{d}\,\mathrm{P}_{2m}(x)}{\mathrm{d}\,x}\mathrm{P}_{2n}(x)(1-x^2)\mathrm{d}x\,. \tag{A1}$$

According to the relations between the Legendre polynomial $\mathrm{P}_{\mu}(\cdot)$ and the associated Legendre function $\mathrm{P}_{\mu}^{\nu}(\cdot)$ (Eq. (4.4.1) in Ref. 36)

$$\mathrm{P}_{\mu}^{\nu}(x)=(-1)^{\nu}(1-x^2)^{\nu/2}\frac{\mathrm{d}^{\nu}}{\mathrm{d}\,x^{\nu}}\mathrm{P}_{\mu}(x)\,, \tag{A2}$$

and the definite integral of triple associated Legendre functions (Eq. (11) in Ref. 37)

$$\begin{aligned}\int_{-1}^{1}\mathrm{P}_{\mu_1}^{\nu_1}(x)\mathrm{P}_{\mu_2}^{\nu_2}(x)\mathrm{P}_{\mu_3}^{\nu_3}(x)\mathrm{d}x=2(-1)^{\nu_3}&\begin{pmatrix}\mu_1 & \mu_2 & \mu_3\\ 0 & 0 & 0\end{pmatrix}\begin{pmatrix}\mu_1 & \mu_2 & \mu_3\\ \nu_1 & \nu_2 & -\nu_3\end{pmatrix}\\ &\times\sqrt{\frac{(\mu_1+\nu_1)!(\mu_2+\nu_2)!(\mu_3+\nu_3)!}{(\mu_1-\nu_1)!(\mu_2-\nu_2)!(\mu_3-\nu_3)!}}\,,\end{aligned} \tag{A3}$$

the integral Eq. (A1) can be obtained as

$$I(l,m,n)=-2\begin{pmatrix}2l & 2m & 2n\\ 0 & 0 & 0\end{pmatrix}\begin{pmatrix}2l & 2m & 2n\\ -1 & 1 & 0\end{pmatrix}\sqrt{4lm(2l+1)(2m+1)}\,, \tag{A4}$$

where the first Wigner 3*j* symbol can be calculated with Eq. (20) in Ref. 21, and the second one can be rewritten by using the symmetric relations as

$$\begin{pmatrix}2l & 2m & 2n\\ -1 & 1 & 0\end{pmatrix}=-\begin{pmatrix}2n & 2m & 2l\\ 0 & 1 & -1\end{pmatrix}=-\begin{pmatrix}2n & 2m & 2l\\ 0 & -1 & 1\end{pmatrix}. \tag{A5}$$

By setting $m_1 = m_2 = m_3 = 0$ in Eq. (9a) of Ref. 38, one obtains the recurrence relation

$$C(1)\begin{pmatrix}2n & 2m & 2l\\ 0 & 1 & -1\end{pmatrix}+D(0)\begin{pmatrix}2n & 2m & 2l\\ 0 & 0 & 0\end{pmatrix}+C(0)\begin{pmatrix}2n & 2m & 2l\\ 0 & -1 & 1\end{pmatrix}=0\,, \tag{A6}$$

where C and D are obtained by Eqs. (9b) and (9c) of Ref. 38 as

$$\begin{cases}C(0)=C(1)=\sqrt{4lm(2l+1)(2m+1)}\\ D(0)=2l(2l+1)+2m(2m+1)-2n(2n+1)\end{cases}. \tag{A7}$$

By substituting Eq. (A7) into Eq. (A6), the second Wigner 3*j* symbol can be represented by the first one. Finally, the integral Eq. (A1) is reduced to

$$I(l,m,n) = 2[l(2l+1)+m(2m+1)-n(2n+1)]\begin{pmatrix} 2l & 2m & 2n \\ 0 & 0 & 0 \end{pmatrix}^2. \tag{A8}$$

REFERENCES

[1] W. S. Gan, J. Yang, and T. Kamakura, “A review of parametric acoustic array in air,” Appl. Acoust. **73**(12), 1211-1219 (2012).

[2] K. Tanaka, C. Shi, and Y. Kajikawa, “Binaural active noise control using parametric array loudspeakers,” Appl. Acoust. **116**, 170-176 (2017).

[3] B. Castagnède, A. Moussatov, D. Lafarge, and M. Saeid, “Low frequency in situ metrology of absorption and dispersion of sound absorbing porous materials based on high power ultrasonic non-linearly demodulated waves,” Appl. Acoust. **69**(7), 634-648 (2008).

[4] E. Skinner, M. Groves, and M. K. Hinders, “Demonstration of a length limited parametric array,” Appl. Acoust. **148**, 423-433 (2019).

[5] K. Rudd and M. Hinders, “Simulation of incident nonlinear sound beam and 3D scattering from complex targets,” J. Comput. Acoust. **16**(03), 427-445 (2008).

[6] C. Shi and W.-S. Gan, “Grating lobe elimination in steerable parametric loudspeaker,” IEEE Trans. Ultrason. Ferroelectr. Freq. Control. **58**(2), 437-450 (2011).

[7] M. Arnela, O. Guasch, P. Sánchez-Martín, J. Camps, R. Alsina-Pagès, and C. Martínez-Suquía, “Construction of an omnidirectional parametric loudspeaker consisting in a sphericaldistribution of ultrasound transducers,” Sensors **18**(12), 4317 (2018).

[8] K. G. Foote, “Discriminating between the nearfield and the farfield of acoustic transducers,” J. Acoust. Soc. Am. **136**(4), 1511-1517 (2014).

[9] P. J. Westervelt, “Parametric acoustic array,” J. Acoust. Soc. Am. **35**(4), 535-537 (1963).

[10] H. Berktay, “Possible exploitation of non-linear acoustics in underwater transmitting applications,” J. Sound Vib. **2**(4), 435-461 (1965).

[11] H. O. Berktay and D. J. Leahy, “Farfield performance of parametric transmitters,” J. Acoust. Soc. Am. **55**(3), 539-546 (1974).

[12] C. Shi and Y. Kajikawa, “Volterra model of the parametric array loudspeaker operating at ultrasonic frequencies,” J. Acoust. Soc. Am. **140**(5), 3643-3650 (2016).

[13] C. Shi and W.-S. Gan, “Product directivity models for parametric loudspeakers,” J. Acoust. Soc. Am. **131**(3), 1938-1945 (2012).

[14] C. Shi and Y. Kajikawa, “A convolution model for computing the far-field directivity of a parametric loudspeaker array,” J. Acoust. Soc. Am. **137**(2), 777-784 (2015).

[15] O. Guasch and P. Sánchez-Martín, “Far-field directivity of parametric loudspeaker arrays

set on curved surfaces," Applied Mathematical Modelling **60**, 721-738 (2018).

[16] R. H. Mellen and M. B. Moffett, "A numerical method for calculating the nearfield of a parametric acoustic source," J. Acoust. Soc. Am. **63**(5), 1622-1624 (1978).

[17] M. B. Moffett and R. H. Mellen, "Nearfield characteristics of parametric acoustic sources," J. Acoust. Soc. Am. **69**(2), 404-409 (1981).

[18] S. I. Aanonsen, T. Barkve, J. N. Tjøtta, and S. Tjøtta, "Distortion and harmonic generation in the nearfield of a finite amplitude sound beam," J. Acoust. Soc. Am. **75**(3), 749-768 (1984).

[19] M. Červenka and M. Bednařík, "A versatile computational approach for the numerical modelling of parametric acoustic array," J. Acoust. Soc. Am. **146**(4), 2163-2169 (2019).

[20] J. Zhong, R. Kirby, and X. Qiu, "A non-paraxial model for the audio sound behind a non-baffled parametric array loudspeaker (L)," J. Acoust. Soc. Am. **147**(3), 1577-1580 (2020).

[21] J. Zhong, R. Kirby, and X. Qiu, "A spherical expansion for audio sounds generated by a circular parametric array loudspeaker," J. Acoust. Soc. Am. **147**(5), 3502-3510 (2020).

[22] M. Červenka and M. Bednařík, "Non-paraxial model for a parametric acoustic array," J. Acoust. Soc. Am. **134**(2), 933-938 (2013).

[23] J. Zhong, S. Wang, R. Kirby, and X. Qiu, "Insertion loss of a thin partition for audio sounds generated by a parametric array loudspeaker," J. Acoust. Soc. Am. **148**(1), 226-235 (2020).

[24] M. F. Hamilton and D. T. Blackstock, *Nonlinear Acoustics* (Acoustical Society of America, New York, 2008).

[25] Y. Kagawa, T. Tsuchiya, T. Yamabuchi, H. Kawabe, and T. Fujii, "Finite element simulation of non-linear sound wave propagation," J. Sound Vib. **154**(1), 125-145 (1992).

[26] H. Nomura, C. M. Hedberg, and T. Kamakura, "Numerical simulation of parametric sound generation and its application to length-limited sound beam," Appl. Acoust. **73**(12), 1231-1238 (2012).

[27] H. E. Bass, L. C. Sutherland, A. J. Zuckerwar, D. T. Blackstock, and D. M. Hester, "Atmospheric absorption of sound: Further developments," J. Acoust. Soc. Am. **97**(1), 680-683 (1995).

[28] G. T. Silva and A. Bandeira, "Difference-frequency generation in nonlinear scattering of acoustic waves by a rigid sphere," Ultrasonics **53**(2), 470-478 (2013).

[29] A. D. Pierce, *Acoustics: An Introduction to Its Physical Principles and Applications* (Springer Nature, Cham, Switzerland, 2019).

[30] M. Červenka and M. Bednařík, "On the structure of multi-Gaussian beam expansion coefficients," Acta Acust. united Ac. **101**(1), 15-23 (2015).

[31] J. J. Wen and M. A. Breazeale, "A diffraction beam field expressed as the superposition of Gaussian beams," J. Acoust. Soc. Am. **83**(5), 1752-1756 (1988).

[32] T. D. Mast and F. Yu, "Simplified expansions for radiation from a baffled circular piston," J. Acoust. Soc. Am. **118**(6), 3457-3464 (2005).

[33] M. A. Poletti, "Spherical expansions of sound radiation from resilient and rigid disks with

reduced error," J. Acoust. Soc. Am. **144**(3), 1180-1189 (2018).
[34] A. Messiah, *Quantum Mechanics: Volume II* (North-Holland Publishing Company Amsterdam, 1962).
[35] ISO 9613-1:1993. Acoustics — Attenuation of sound during propagation outdoors — Part 1: Calculation of the absorption of sound by the atmosphere (International Organization for Standardization, Genève, 1993).
[36] S. Zhang and J. Jin, *Computation of Special Functions* (John Wiley & Sons, New York, 1996).
[37] H. A. Mavromatis and R. S. Alassar, "A generalized formula for the integral of three associated Legendre polynomials," Appl. Math. Lett. **12**(3), 101-105 (1999).
[38] K. Schulten and R. G. Gordon, "Exact recursive evaluation of 3 j-and 6 j-coefficients for quantum-mechanical coupling of angular momenta," J. Math. Phys. **16**(10), 1961-1970 (1975).